

Di-Jet Extinction from Non-Perturbative Quantum Gravity Effects

Can Kilic¹, Amitabh Lath², Keith Rose², Scott Thomas²

¹*Theory Group, Department of Physics and Texas Cosmology Center
The University of Texas at Austin
Austin, TX 78712*

²*Department of Physics
Rutgers University
Piscataway, NJ 08854*

Abstract

We study a novel signature of TeV scale quantum gravity that manifests itself as an extinction of hard short distance scattering in QCD processes. The extinction behavior is due to the predominance of high-entropy intermediate states of the underlying quantum gravity theory. We model extinction using a large damping Veneziano form-factor modification of QCD scattering amplitudes that suppresses high p_T scattering. We propose and demonstrate the potential of an LHC search for extinction, with a possible reach for the string scale as high as 3 TeV with 7 TeV LHC collision data, and up to 5 TeV from high-statistics 13 TeV data.

1 Introduction

The LHC, currently operating at 8 TeV center of mass energy, and planned to operate at 13 or 14 TeV after the shutdown period beginning at the end of 2012, is exploring new frontiers in short distance physics. Among the most dramatic outcomes of probing physics beyond the TeV scale is the possibility of large extra dimensions [1] where the fundamental Planck scale is exponentially reduced, which may make it possible for the LHC to access states associated with the fundamental properties of gravity at the shortest scales. A reduced Planck scale in the TeV regime can also be realized in theories with warped extra dimensions [2]. Various potential signatures of such a low Planck scale have been considered in several guises [3, 4, 5, 6], including in the form of string Regge resonances [7, 8, 9] when the underlying string theory is weakly coupled, as well as the formation of microscopic black holes [10, 11, 12, 13, 14, 15] in the strongly coupled regime. In this work we wish to emphasize a very different type of signature of strongly coupled TeV scale quantum gravity, which may give the earliest indication of the exotic underlying theory.

Specifically, in realizations of TeV scale gravity based on string theory in a strong coupling regime, a novel feature at center of mass energies comparable to the string scale is the contribution to scattering processes from the exchange of high entropy states. This feature is not specific to any single underlying string theory model but is rather robust. Due to the high entropy of these intermediate states, processes with a small number of final state particles become suppressed [16, 17]. As we will show later in this paper, this effect manifests itself immediately at the string scale, while the production of black holes is expected to be realized only at significantly higher energies. Thus the earliest observable in such a scenario may be the “extinction” of all $2 \rightarrow 2$ processes with center of mass energies of roughly the string scale. In the context of the LHC, this will be observable as an exponential drop in the high- p_T QCD di-jet production. It should also be emphasized that in collider studies of black hole production, the models that are used exhibit a discontinuity as the cross section for black hole formation is taken to jump abruptly from zero to a large geometric cross section at the threshold energy. Extinction on the other hand can be modeled in a way such that the turn-on of the suppression is gradual, and the transition from QCD-like behavior to the extinction regime is smooth.

In the following study, we will model the effects arising from the underlying string theory description as Veneziano type form-factors that modify all $2 \rightarrow 2$ scattering amplitudes in a universal manner. Based on this model, we will then derive the form-factor modified QCD scattering amplitudes for various initial and final states. Apart from studying these modifications analytically, we also implement the modified amplitudes into a matrix-element based Monte Carlo event generation tool and thus perform a realistic collider study of the

extinction phenomenon, and assess the sensitivity of the LHC to a string scale in the TeV regime with early data as well as with large integrated luminosity after the energy upgrade.

2 Modeling Extinction

2.1 Damped Veneziano Scattering Amplitudes

The goal of this section is to model the effects due to the exchange of high-entropy states by a phenomenological low energy description, and then to study the most salient features quantitatively. The idea behind the model is to map the color-ordered helicity amplitudes for any $2 \rightarrow 2$ QCD process on to the corresponding string theory amplitude.

Each string theory amplitude includes the Veneziano form factor

$$V(x, y) = \frac{\Gamma(1-x)\Gamma(1-y)}{\Gamma(1-x-y)} \quad (1)$$

where x, y are kinematic invariants derived from the momenta associated with neighboring operators (as defined below).

To match this behavior, the color ordered helicity amplitudes for external states with momenta p_1, p_2, p_3, p_4 are taken to be those of QCD modified by the Veneziano form factor in adjacent kinematic channels in the color ordered amplitude

$$\mathcal{A}(p_1, p_2, p_3, p_4) = \mathcal{A}(p_1, p_2, p_3, p_4)_{\text{QCD}} \tilde{V}(x_{12}, x_{23}) \quad (2)$$

where $x_{AB} = (p_A + p_B)^2 = 2p_A \cdot p_B$ with all momenta incoming and

$$\tilde{V}(x, y) = V\left(\frac{x(1+i\alpha)}{M^2}, \frac{y(1+i\alpha)}{M^2}\right). \quad (3)$$

Here M is the mass scale for the form factor modification, and α is a dimensionless damping parameter discussed below. The form factor approaches unity for small invariant momenta, $\tilde{V}(0, 0) = 1$, so the scattering amplitudes smoothly reduce to QCD at fixed momenta in the limit of large mass scale

$$\lim_{M \rightarrow \infty} \mathcal{A}(p_1, p_2, p_3, p_4) = \mathcal{A}(p_1, p_2, p_3, p_4)_{\text{QCD}} \quad (4)$$

Let us now derive the form-factor modified amplitudes for all QCD processes, organized by different choices of external states.

2.1.1 Two Quarks of One Flavor and Two Quarks of Another Flavor

The unique color ordered helicity amplitudes with two quarks of one flavor and two quarks of another flavor may be written

$$\mathcal{A}(\bar{q}_1^{-i}, q_2^{+j}, \bar{q}_3^{\pm k}, q_4^{\mp \ell}) = A(\bar{q}_1^{-i}, q_2^{+j}, \bar{q}_3^{\pm k}, q_4^{\mp \ell}) (T^a)_j^i (T^a)_\ell^k \quad (5)$$

with others related by charge conjugation or parity, where throughout helicity and momentum indicated in helicity amplitudes are all incoming. The i, j, \dots are (anti)fundamental indices, a, b, \dots are adjoint indices, and T^a are fundamental generators of $SU(3)_C$ with normalization $\text{Tr}(T^a T^b) = \delta^{ab}$. The QCD helicity amplitudes with color factors stripped off, written in terms of twistor products are related by permutations to a single amplitude

$$A(\bar{q}_1^{-i}, q_2^{+j}, \bar{q}_3^{-k}, q_4^{+\ell})_{\text{QCD}} = g^2 \frac{[13]\langle 42 \rangle}{\langle 12 \rangle [21]} \quad (6)$$

$$A(\bar{q}_1^{-i}, q_2^{+j}, \bar{q}_3^{+k}, q_4^{-\ell})_{\text{QCD}} = g^2 \frac{[14]\langle 32 \rangle}{\langle 12 \rangle [21]} \quad (7)$$

where the twistor products are defined in terms of contractions of the wave function spinors by $[AB] \equiv \chi^\alpha(p_A) \chi_\alpha(p_B)$ and $\langle AB \rangle \equiv \chi_{\dot{\alpha}}^*(p_A) \chi^{\dot{\alpha}}(p_B)$ and satisfy $\langle AB \rangle = -\langle BA \rangle$, $\langle AB \rangle^* = [BA]$. These color ordered helicity amplitudes may be averaged (summed) over initial (final) state color and helicity configurations to give the averaged squared matrix elements for $2 \rightarrow 2$ scattering processes involving two quarks of one flavor and two of another flavor with the form factor modification

$$\langle |\mathcal{A}(q_1 \bar{q}_2 \rightarrow q'_3 \bar{q}'_4)|^2 \rangle = g^4 \frac{4}{9} \frac{u^2 + t^2}{s^2} |\tilde{V}(s, t)|^2 \quad (8)$$

$$\langle |\mathcal{A}(q_1 q'_2 \rightarrow q_3 q'_4)|^2 \rangle = g^4 \frac{4}{9} \frac{s^2 + u^2}{t^2} |\tilde{V}(t, u)|^2 \quad (9)$$

$$\langle |\mathcal{A}(q_1 \bar{q}'_2 \rightarrow q_3 \bar{q}'_4)|^2 \rangle = g^4 \frac{4}{9} \frac{s^2 + u^2}{t^2} |\tilde{V}(s, t)|^2 \quad (10)$$

$$\langle |\mathcal{A}(\bar{q}_1 \bar{q}'_2 \rightarrow \bar{q}_3 \bar{q}'_4)|^2 \rangle = g^4 \frac{4}{9} \frac{s^2 + u^2}{t^2} |\tilde{V}(t, u)|^2 \quad (11)$$

where $\langle AB \rangle [BA] = x_{AB}$, and $s = x_{12} = x_{34}$, $t = x_{13} = x_{24}$, and $u = x_{14} = x_{23}$ are the Mandelstam variables for the scattering order $12 \rightarrow 34$ indicated in the squared matrix elements. Each scattering matrix element squared (8-11) includes a sum over two independent helicity channels (not related by parity) of single helicity amplitudes squared in a single color channel.

2.1.2 Four Quarks of the Same Flavor

The color ordered helicity amplitudes with four quarks of the same flavor with either all the chiralities the same or two of one chirality and two of the other may be written respectively

$$\mathcal{A}(\bar{q}_1^{-i}, q_2^{+j}, \bar{q}_3^{-k}, q_4^{+\ell}) = A(\bar{q}_1^{-i}, q_2^{+j}, \bar{q}_3^{-k}, q_4^{+\ell}) (T^a)_j^i (T^a)_\ell^k \quad (12)$$

$$\mathcal{A}(\bar{q}_1^{-i}, q_2^{-j}, \bar{q}_3^{+k}, q_4^{+\ell}) = A(\bar{q}_1^{-i}, q_2^{-j}, \bar{q}_3^{+k}, q_4^{+\ell}) (T^a)_j^i (T^a)_\ell^k \quad (13)$$

with others related by charge conjugation or parity. The QCD helicity amplitudes in this case with the color factor stripped off are identical to the amplitudes (6) and (7). These color ordered helicity amplitudes may be averaged (summed) over initial (final) state color and helicity configurations to give the the averaged matrix elements squared for $2 \rightarrow 2$ scattering processes involving four quarks of a single flavor with the form factor modification

$$\langle |\mathcal{A}(q_1 \bar{q}_2 \rightarrow q_3 \bar{q}_4)|^2 \rangle = g^4 \frac{4}{9} \left[\frac{u^2 + t^2}{s^2} + \frac{s^2 + u^2}{t^2} - \frac{2}{3} \frac{u^2}{st} \right] |\tilde{V}(s, t)|^2 \quad (14)$$

$$\langle |\mathcal{A}(q_1 q_2 \rightarrow q_3 q_4)|^2 \rangle = g^4 \frac{4}{9} \left[\frac{s^2 + u^2}{t^2} + \frac{s^2 + t^2}{u^2} - \frac{2}{3} \frac{s^2}{tu} \right] |\tilde{V}(t, u)|^2 \quad (15)$$

$$\langle |\mathcal{A}(\bar{q}_1 \bar{q}_2 \rightarrow \bar{q}_3 \bar{q}_4)|^2 \rangle = g^4 \frac{4}{9} \left[\frac{s^2 + u^2}{t^2} + \frac{s^2 + t^2}{u^2} - \frac{2}{3} \frac{s^2}{tu} \right] |\tilde{V}(t, u)|^2 \quad (16)$$

Each scattering matrix element squared (14-16) contains two types of terms. The first type for two quarks of one chirality and two of the other chirality includes a sum over two independent helicity channels (not related by parity) of single helicity amplitudes squared in a single color channel. The second type for four quarks of the same chirality includes a sum over the same two independent helicity channels of the square of a coherent sum of two helicity amplitudes in different color channels.

2.1.3 Four Gluons

The unique four gluon color ordered helicity amplitudes may be written

$$\mathcal{A}(g_1^{-a}, g_2^{+b}, g_3^{\pm c}, g_4^{\mp d}) = A(g_1^-, g_2^+, g_3^\pm, g_4^\mp) \text{Tr}(T^a T^b T^c T^d) \quad (17)$$

$$\mathcal{A}(g_1^{-a}, g_2^{-b}, g_3^{+c}, g_4^{+d}) = A(g_1^-, g_2^-, g_3^+, g_4^+) \text{Tr}(T^a T^b T^c T^d) \quad (18)$$

with others related by parity. The QCD helicity amplitudes with color factors stripped off are all related by permutations to the Parke-Taylor amplitude [18]

$$A(g_1^-, g_2^+, g_3^+, g_4^-)_{\text{QCD}} = g^2 \frac{\langle 14 \rangle^4}{\langle 12 \rangle \langle 23 \rangle \langle 34 \rangle \langle 41 \rangle} \quad (19)$$

$$A(g_1^-, g_2^+, g_3^-, g_4^+)_{\text{QCD}} = g^2 \frac{\langle 13 \rangle^4}{\langle 12 \rangle \langle 23 \rangle \langle 34 \rangle \langle 41 \rangle} \quad (20)$$

$$A(g_1^-, g_2^-, g_3^+, g_4^+)_{\text{QCD}} = g^2 \frac{\langle 12 \rangle^4}{\langle 12 \rangle \langle 23 \rangle \langle 34 \rangle \langle 41 \rangle} \quad (21)$$

These color ordered helicity amplitudes may be averaged (summed) over initial (final) state color and helicity configurations to give the the averaged matrix elements squared for $2 \rightarrow 2$ scattering processes involving four gluons with the form factor modification

$$\begin{aligned} \langle |\mathcal{A}(g_1 g_2 \rightarrow g_3 g_4)|^2 \rangle = g^4 \frac{9}{4} \left(\frac{1}{s^2} + \frac{1}{t^2} + \frac{1}{u^2} \right) & \left[s^2 |\tilde{V}(t, u)|^2 + t^2 |\tilde{V}(s, u)|^2 + u^2 |\tilde{V}(s, t)|^2 \right. \\ & \left. - \frac{4}{27} |s \tilde{V}(t, u) + t \tilde{V}(s, u) + u \tilde{V}(s, t)|^2 \right] \quad (22) \end{aligned}$$

The scattering matrix element squared (22) includes a sum over three independent helicity channels (not related by parity) of the square of a coherent sum of three helicity amplitudes each in a different color channel.

2.1.4 Two Quarks and two Gluons

The unique color ordered helicity amplitudes for two quarks of a given flavor and chirality and two gluons may be written

$$\mathcal{A}(\bar{q}_1^{-i}, q_2^{+j}, g_3^{\pm a}, g_4^{\mp b}) = A(\bar{q}_1^-, q_2^+, g_3^\pm, g_4^\mp) (T^a T^b)_j^i \quad (23)$$

with others related by charge conjugation or parity. The QCD helicity amplitudes with color factors stripped off are all related by permutations to a single amplitude

$$A(\bar{q}_1^-, q_2^+, g_3^+, g_4^-)_{\text{QCD}} = g^2 \frac{\langle 14 \rangle^3 \langle 24 \rangle}{\langle 12 \rangle \langle 23 \rangle \langle 34 \rangle \langle 41 \rangle} \quad (24)$$

$$A(\bar{q}_1^-, q_2^+, g_3^-, g_4^+)_{\text{QCD}} = g^2 \frac{\langle 13 \rangle^3 \langle 23 \rangle}{\langle 12 \rangle \langle 23 \rangle \langle 34 \rangle \langle 41 \rangle} \quad (25)$$

These color ordered helicity amplitudes may be averaged (summed) over initial (final) state color and helicity configurations to give the the averaged matrix elements squared for $2 \rightarrow 2$ scattering processes involving two quarks of a given flavor and two gluons with the form factor modification

$$\langle |\mathcal{A}(q_1 \bar{q}_2 \rightarrow g_3 g_4)|^2 \rangle = g^4 \frac{32}{27} \frac{u^2 + t^2}{s^2} \left[\frac{u}{t} |\tilde{V}(s, t)|^2 + \frac{t}{u} |\tilde{V}(s, u)|^2 - \frac{1}{4} \text{Re}(\tilde{V}(s, t) \tilde{V}^*(s, u)) \right] \quad (26)$$

$$\langle |\mathcal{A}(g_1 g_2 \rightarrow q_3 \bar{q}_4)|^2 \rangle = g^4 \frac{1}{6} \frac{u^2 + t^2}{s^2} \left[\frac{u}{t} |\tilde{V}(s, t)|^2 + \frac{t}{u} |\tilde{V}(s, u)|^2 - \frac{1}{4} \text{Re}(\tilde{V}(s, t) \tilde{V}^*(s, u)) \right] \quad (27)$$

$$\langle |\mathcal{A}(q_1 g_2 \rightarrow q_3 g_4)|^2 \rangle = g^4 \frac{4}{9} \frac{s^2 + u^2}{t^2} \left[-\frac{s}{u} |\tilde{V}(t, u)|^2 - \frac{u}{s} |\tilde{V}(s, t)|^2 + \frac{1}{4} \text{Re}(\tilde{V}(s, t) \tilde{V}^*(t, u)) \right] \quad (28)$$

$$\langle |\mathcal{A}(\bar{q}_1 g_2 \rightarrow \bar{q}_3 g_4)|^2 \rangle = g^4 \frac{4}{9} \frac{s^2 + u^2}{t^2} \left[-\frac{s}{u} |\tilde{V}(t, u)|^2 - \frac{u}{s} |\tilde{V}(s, t)|^2 + \frac{1}{4} \text{Re}(\tilde{V}(s, t) \tilde{V}^*(t, u)) \right] \quad (29)$$

Each scattering matrix element squared (26-29) includes a sum over two independent helicity channels (not related by parity) of the square of a coherent sum of two helicity amplitudes in different color channels.

2.2 Quantitative Behavior of the Form Factor

Unlike the case of the form factor with a small imaginary part, which leads to resonance-like behavior corresponding to string Regge excitations, in the case of complex argument, the form factor leads to exponential suppression. As we have discussed in the introduction, this is the correct behavior we expect from the presence of high-entropy intermediate states. The asymptotic behavior of the form factor can be easily illustrated using Stirling's approximation for the gamma-function

$$\Gamma(z) \approx \sqrt{2\pi z}^{\frac{z-1}{2}} e^{-z}. \quad (30)$$

Using the form-factor modified amplitudes listed in section 2.1, we illustrate the effect of extinction for several processes for central scattering ($u = t = -\frac{s}{2}$) in figure 1. What is plotted here is the suppression relative to QCD, given by

$$\frac{|\mathcal{M}|^2}{|\mathcal{M}|_{QCD}^2}. \quad (31)$$

It is straightforward to check that for exactly central scattering, the suppression of all QCD processes listed in the appendix coincide with one of the four curves shown in figure 1. It is easy to see on this figure that the suppression becomes very significant as soon as the center-of-mass energy of the collision becomes larger than the scale M .

Of course, not all collisions at the LHC are central, so let us study the behavior of the form factor over the whole kinematic region. This will in fact point the way for choosing a good kinematic variable in which to bin the data and obtain good sensitivity to the extinction behavior. The $2 \rightarrow 2$ process that dominates the cross section at high energy (with or without the form-factor modification) is $qg \rightarrow qg$ so the behavior of the form factor for this process is a good approximation to the behavior for the sum of all $2 \rightarrow 2$ processes. The suppression of $qg \rightarrow qg$ as a function of scattering angle and center-of-mass energy is shown in figure 2. The black contours correspond to the log-base-10 of the suppression

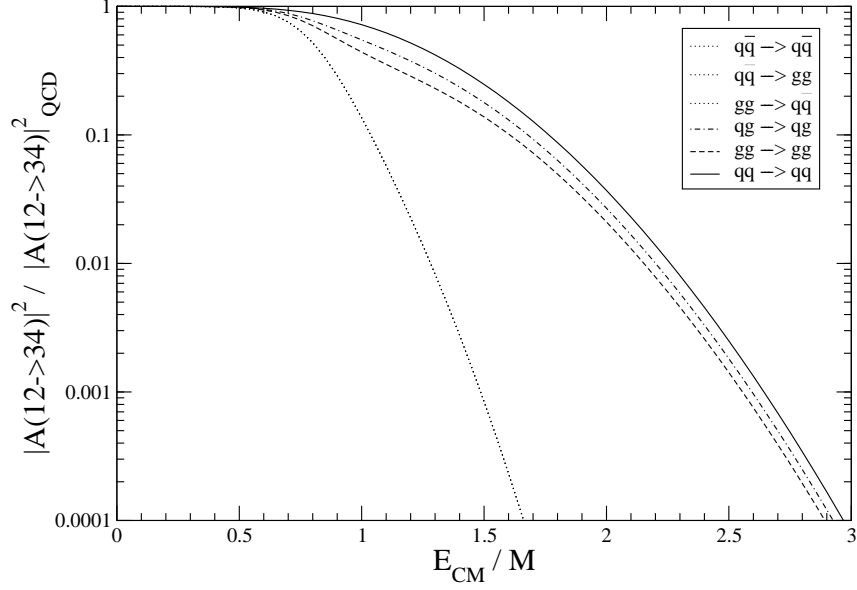


Figure 1: Effect of the Veneziano form factor extinction with $\alpha = 1$ on various $2 \rightarrow 2$ quark and gluon scattering probabilities for central scattering $u = t = -s/2$ as a function of the center-of-mass energy.

factor as defined in eq. (31), as do the negative numbers labeling these contours, i.e. the contour labeled “-1” shows where the suppression is equal to 0.1 etc. We overlay on top of this the contours of constant p_T^2 , illustrated with the red contours, and the positive numbers labeling them in units of M^2 . We see that there is relatively good alignment between the contours of constant suppression and those of constant p_T . This indicates that p_T will be a good variable for binning the data, such that one is maximally sensitive to the effects of extinction.

3 LHC Analysis

3.1 Monte Carlo Implementation

In order to study the effects of extinction at the LHC, we incorporate the form-factor-modified amplitudes into Pythia 6.4 [19]. Specifically, we modify the hard-scattering matrix elements occurring in the subroutine PYSGQC. With this modification we are able to generate events corresponding to the extinction scenario, and interface them to the (unmodified) parton shower and hadronization subroutines of Pythia.

Since extinction is primarily an effect on large-angle scattering, we only generate hard scattering events within a pseudorapidity range of $|\eta| < 1.5$. Furthermore, in order to

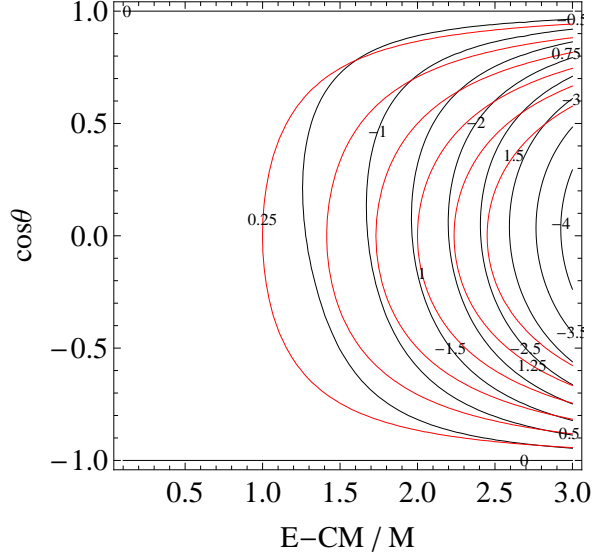


Figure 2: Effect of the Veneziano form factor extinction with $\alpha = 1$ on the $qq \rightarrow qq$ scattering probability as a function of the center of mass scattering angle and center of mass energy. Black contours indicate $|\mathcal{A}(qq \rightarrow qq)|^2/|\mathcal{A}(qq \rightarrow qq)|_{\text{QCD}}^2$ labeled in \log_{10} units. Red contours indicate $p_T^2/M^2 = (s/4)(1 - \cos^2 \theta)/M^2$ in equal intervals.

achieve high statistics in the large center-of-mass energy regime, we generate events in bins of \sqrt{s} and combine the samples weighted by their relative cross sections.

We also pass the resulting events through PGS [20] in order to account for detector effects such as acceptance and jet energy resolution. We use the CMS parameter set of PGS, with a jet definition based on a cone algorithm with $\Delta R = 0.7$.

3.2 Search Strategy

Having demonstrated in section 2.2 that the form-factor suppression is well aligned with contours of p_T , we will use histograms of p_T in order to study the effects of extinction. Specifically, as our event selection criteria we demand that there are two hard jets in the event, both with $p_T > 200$ GeV and $|\eta| < 1.5$.

Our analysis will be focused on evaluating the statistical significance with which models of extinction with various choices for the scale M can be distinguished from QCD. Clearly this should not be taken as a realistic estimate of the reach until various sources of systematic uncertainty can also be included, such as PDF uncertainties and modifications of differential cross sections due to next to leading order effects. However, higher order calculations for $2 \rightarrow 2$ processes in the presence of quantum gravity effects are not currently

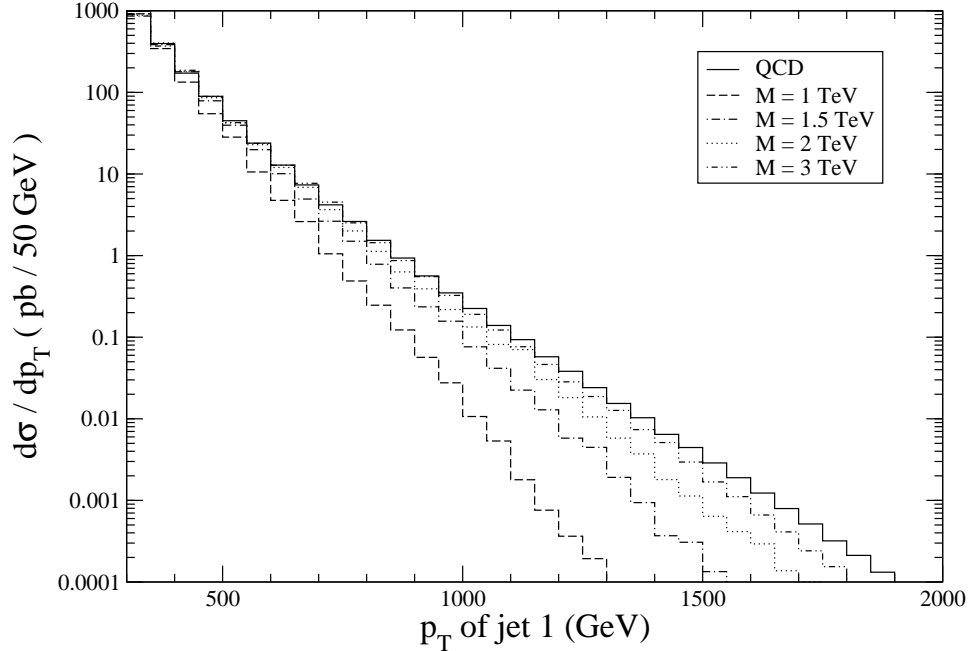


Figure 3: The differential cross section as a function of the p_T of the hardest jet at 7 TeV after the selection cuts described in the text.

available, and the same is also true for even leading order calculations of $2 \rightarrow 3$ or higher multiplicity matrix elements. Therefore, currently an apples-to-apples comparison of QCD to extinction can only be performed at leading order. A comparison of extinction based on leading order matrix elements vs. next to leading order QCD is not recommended, as the extinction matrix elements are direct modifications of the QCD matrix elements by the form factor, therefore it would not be possible to model NLO QCD and extinction based on LO QCD such that they agree at low energies. In any case, since we are unable to account for such systematic uncertainties, our results should not be taken as precise statements about the LHC reach of an extinction search, but rather as a preliminary check that an extinction search is at least viable, even if the significance may be reduced by systematic effects. It should be noted that the log-likelihood analysis we will describe shortly relies on shape information only, therefore it is insensitive to at least certain types of systematic effects such as the scaling of the cross section by a constant k-factor.

We thus proceed to assess the sensitivity of the LHC to extinction with the full 7 TeV dataset of 5 fb^{-1} , and with a future high-statistics sample of 100 fb^{-1} at 13 TeV. For the 7 TeV study, we generate QCD events in \sqrt{s} bins of 300 GeV, starting at $\sqrt{s} = 200 \text{ GeV}$, each bin containing 50000 events, which correspond to high statistics at the high end of the p_T spectrum where we will perform our statistical analysis. We use the same \sqrt{s} bins

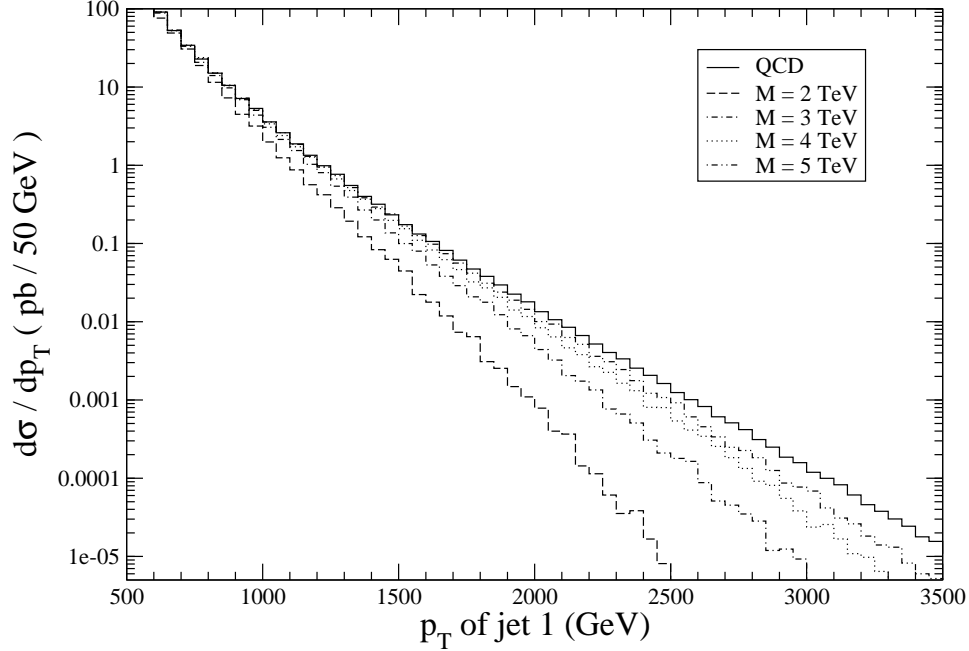


Figure 4: The differential cross section as a function of the p_T of the hardest jet at 13 TeV after the selection cuts described in the text.

to simulate extinction with the scale M chosen at 1 TeV, 1.5 TeV, 2 TeV and 3 TeV, with 25000 events in each bin, which is very high statistics considering the sharp decrease of extinction cross sections at high p_T . The p_T spectrum of the hardest jet in each event are shown in figure 3.

For the 13 TeV samples, we use bins of \sqrt{s} of 500 GeV starting at 500 GeV, with 100000 events in each bin for QCD, and 25000 events per bin for extinction samples with a string scale of 2 TeV, 3 TeV, 4 TeV and 5 TeV. The p_T spectrum of the hardest jet in each event is shown in figure 4.

3.3 Results

We proceed to estimate the statistical significance with which the extinction scenario can be distinguished from QCD by setting up a log-likelihood analysis as follows. We divide the p_T spectra shown in figures 3 and 4 in 100 GeV bins above $p_T = 500$ GeV for the 7 TeV data and above $p_T = 1.5$ TeV for the 13 TeV data. Using the cross section information in these bins we define the probability distributions for both the QCD hypothesis

$$p_i^{\text{QCD}} = \frac{\sigma_i^{\text{QCD}}}{\sum_{\text{bins}} \sigma_i^{\text{QCD}}} \quad (32)$$

as well as the extinction hypothesis defined in the same way. Note that the overall normalization cancels out such that the p_i are sensitive to shape only.

For each of the two competing hypotheses (QCD and extinction with a specific choice of the scale M) we perform 50000 pseudoexperiments based on these probability distributions, where the number of events per pseudoexperiment is chosen with a Poisson distribution around the mean number of expected events for that hypothesis. For each pseudoexperiment, the number of events in each bin is then used to define the log-likelihood ratio

$$\mathcal{L}(\{N_i\}) = 2\text{Log} \left(\frac{\prod_i (p_i^{\text{EXT}})^{N_i}}{\prod_i (p_i^{\text{QCD}})^{N_i}} \right). \quad (33)$$

Integrating the probability under the log-likelihood distributions of the two hypotheses past the point where the two distributions intersect, we extract the p-value with which the two hypotheses can be distinguished. In both cases we find p-values that are below 5.7×10^{-7} which corresponds to 5σ significance. Of course, as we mentioned before, in the absence of a more realistic treatment of systematic uncertainties, this result should only be taken as a first check for the plausibility of such a search.

4 Conclusions

We have pointed to a novel signature of low scale quantum gravity, which manifests itself as a sharp decrease in all scattering processes with large transverse momenta. We have modeled this phenomenon by using form-factor modified QCD amplitudes based on underlying string theory considerations, where all scattering amplitudes are proportional to the Veneziano form factor. In order to model the behavior of the underlying theory in a regime of strong coupling, we have evaluated the form factors with large values of the damping parameter α , thus giving rise to the expected behavior of exponential suppression at large p_T . We have performed a collider analysis of the extinction in order to assess the LHC sensitivity to such a scenario. Using a log-likelihood analysis based on statistical uncertainties only, we expect that a string scale of 3 TeV may be distinguished from QCD using the 7 TeV data sample, and with 100 fb^{-1} of integrated luminosity at 13 TeV this can increase to a string scale of 5 TeV.

While future work is needed in order to include the effects of systematic uncertainties into this analysis and thus obtain a realistic estimate for the reach, this study shows that a search for extinction looks promising as a first indication of low scale quantum gravity at the LHC.

Acknowledgments

We would like to thank J.P Chou for useful comments. This research was supported in part by DOE grant DE-FG02-96ER40959 and NSF Grant PHY-0969020.

References

- [1] N. Arkani-Hamed, S. Dimopoulos and G. R. Dvali, “The Hierarchy problem and new dimensions at a millimeter,” Phys. Lett. B **429**, 263 (1998) [hep-ph/9803315].
- [2] L. Randall and R. Sundrum, “A Large mass hierarchy from a small extra dimension,” Phys. Rev. Lett. **83**, 3370 (1999) [hep-ph/9905221].
- [3] I. Antoniadis, N. Arkani-Hamed, S. Dimopoulos and G. R. Dvali, “New dimensions at a millimeter to a Fermi and superstrings at a TeV,” Phys. Lett. B **436**, 257 (1998) [hep-ph/9804398].
- [4] G. F. Giudice, R. Rattazzi and J. D. Wells, “Quantum gravity and extra dimensions at high-energy colliders,” Nucl. Phys. B **544**, 3 (1999) [hep-ph/9811291].
- [5] E. A. Mirabelli, M. Perelstein and M. E. Peskin, “Collider signatures of new large space dimensions,” Phys. Rev. Lett. **82**, 2236 (1999) [hep-ph/9811337].
- [6] D. Lust, S. Stieberger and T. R. Taylor, “The LHC String Hunter’s Companion,” Nucl. Phys. B **808**, 1 (2009) [arXiv:0807.3333 [hep-th]].
- [7] S. Cullen, M. Perelstein and M. E. Peskin, “TeV strings and collider probes of large extra dimensions,” Phys. Rev. D **62**, 055012 (2000) [hep-ph/0001166].
- [8] S. Chatrchyan *et al.* [CMS Collaboration], “Search for Resonances in the Dijet Mass Spectrum from 7 TeV pp Collisions at CMS,” Phys. Lett. B **704**, 123 (2011) [arXiv:1107.4771 [hep-ex]].
- [9] G. Aad *et al.* [ATLAS Collaboration], “Search for New Physics in the Dijet Mass Distribution using 1 fb⁻¹ of pp Collision Data at sqrt(s) = 7 TeV collected by the ATLAS Detector,” Phys. Lett. B **708**, 37 (2012) [arXiv:1108.6311 [hep-ex]].
- [10] T. Banks and W. Fischler, “A Model for High-Energy Scattering in Quantum Gravity,” hep-th/9906038.
- [11] S. B. Giddings and S. D. Thomas, “High-Energy Colliders as Black Hole Factories: The End of Short Distance Physics,” Phys. Rev. D **65**, 056010 (2002) [hep-ph/0106219].

- [12] S. Dimopoulos and G. L. Landsberg, “Black holes at the LHC,” *Phys. Rev. Lett.* **87**, 161602 (2001) [hep-ph/0106295].
- [13] P. Meade and L. Randall, “Black Holes and Quantum Gravity at the LHC,” *JHEP* **0805**, 003 (2008) [arXiv:0708.3017 [hep-ph]].
- [14] [ATLAS Collaboration], ATLAS-CONF-2011-068.
- [15] S. Chatrchyan *et al.* [CMS Collaboration], “Search for microscopic black holes in pp collisions at $\sqrt{s} = 7$ TeV,” *JHEP* **1204**, 061 (2012) [arXiv:1202.6396 [hep-ex]].
- [16] D. J. Gross and P. F. Mende, “The High-Energy Behavior of String Scattering Amplitudes,” *Phys. Lett. B* **197**, 129 (1987).
- [17] D. J. Gross and P. F. Mende, “String Theory Beyond the Planck Scale,” *Nucl. Phys. B* **303**, 407 (1988).
- [18] S. J. Parke and T. R. Taylor, “An Amplitude for n Gluon Scattering,” *Phys. Rev. Lett.* **56**, 2459 (1986).
- [19] T. Sjostrand, S. Mrenna, P. Z. Skands, “PYTHIA 6.4 Physics and Manual,” *JHEP* **0605**, 026 (2006). [hep-ph/0603175].
- [20] J. Conway *et al.*, “PGS 4: Pretty Good Simulation of high energy collisions,” 2006, www.physics.ucdavis.edu/~conway/research/software/pgs/pgs4-general.htm